

# Fermi Surface Resonance and Quantum Criticality in Strongly Interacting Fermi Gases

Dmitry Miserev,<sup>1\*</sup> Jelena Klinovaja,<sup>1</sup> and Daniel Loss<sup>1</sup>

<sup>1</sup>*Department of Physics, University of Basel,  
Klingelbergstrasse 82, CH-4056 Basel, Switzerland*

(Dated: July 10, 2020)

Fermions in the Fermi gas obey the Pauli exclusion principle restricting any two fermions from filling the same quantum state. Strong interaction between fermions can completely change the properties of the Fermi gas. In our theoretical study we find a new exotic quantum phase in strongly interacting Fermi gases constrained to a certain condition imposed on the Fermi surfaces which we call the Fermi surface resonance. The new phase is quantum critical which can be identified by the power-law frequency tail of the spectral density and divergent static susceptibilities. An especially striking feature of the new phase is the anomalous power-law temperature dependence of the dc resistivity that is similar to strange metals. The new quantum critical phase can be experimentally found in ordinary semiconductor heterostructures.

**Introduction.** Physical properties of Fermi gases in a large variety of different materials have been extensively studied over the past century [1]. Properties of the non-interacting Fermi gas are entirely determined by single-particle physics and the Fermi statistics [2]. Fermions in condensed matter physics are represented by electrons or holes that interact via the Coulomb force. The Coulomb interaction between fermions can significantly change the properties of a Fermi gas. For example, a one-dimensional Fermi gas forms the strongly correlated Tomonaga-Luttinger liquid at arbitrarily weak interactions [3–5]. In higher spatial dimensions, however, weak interactions do not spoil the properties of Fermi gases but only slightly change the non-interacting characteristics. The gas of such weakly interacting fermions can be modeled by the gas of “dressed” non-interacting Landau quasiparticles. The gas of Landau quasiparticles is known as the Landau Fermi liquid (LFL) [6].

If the interaction is strong, the LFL breaks down and the ground state of the the strongly interacting fermion system can dramatically change. The interaction strength is measured by the dimensionless interaction parameter  $r_s$

$$r_s = \frac{v_C}{E_F} \sim \frac{me^2}{\epsilon n^{1/D}} \quad (1)$$

where  $v_C$  is the Coulomb interaction,  $E_F$  the Fermi energy,  $n$  the fermion density,  $m$  the effective mass,  $e$  the elementary charge,  $\epsilon$  the dielectric constant, and  $D$  the spatial dimension. Thus, in order to drive the system into the strongly interacting regime  $r_s \gg 1$ , we generally need a large effective mass  $m$ , small dielectric constant  $\epsilon$  and small density  $n$ . For example, the strongly interacting electron gas in near magic angle twisted bilayer graphene exhibits exotic magnetism [7], charge density order [8], and unconventional superconductivity [9], because  $r_s \gg 1$  due to the low electron density and large effective mass. The hole-doped semiconductors such as GaAs, InAs, InSb [10], or Ge [11] are also good candidates because of the large effective hole mass. The hole

density  $n$  can be tuned to sufficiently small values by the electrostatic gates. Taking a two-dimensional semiconductor [10] with  $\epsilon = 10$ ,  $m = 0.2m_0$ , where  $m_0$  is the bare electron mass, and  $n = 10^{11} \text{ cm}^{-2}$  we get  $r_s \sim 10 \gg 1$ , which corresponds to the strongly interacting regime.

The Coulomb interaction between charged fermions can be divided into two physically different parts. The first one is the classical electrostatic interaction with other electric charges via the charge density. In quantum physics there is one more type of the interaction which comes from the quantum indistinguishability of two interacting fermions of the same type. This is the exchange interaction [12]. The exchange interaction can mix quasiparticles from different Fermi surfaces. In our study we show that under certain conditions on the Fermi surfaces the exchange interaction mixes the fermions into a new exotic phase. In this new phase the fermions form a strongly interacting quantum liquid and the LFL quasiparticle picture breaks down.

In the absence of quasiparticles there is no simple visual picture to characterize quantum processes. In order to describe quantum liquids with no quasiparticles, the field description is required [13]. Excitations or quanta of the fermion fields in the LFL are long lived and they represent the Landau quasiparticles. The Heisenberg uncertainty principle obliges all physical fields to fluctuate. For example, quantum fluctuations in the LFL result in the finite lifetime of the Landau quasiparticles [14]. However, quantum fluctuations in strongly interacting quantum liquids completely destroy quasiparticles [15]. This means that all field excitations are strongly damped by the quantum fluctuations and cannot be considered as sharply defined long lived quasiparticles. The single-particle methods in such quantum liquids are inadequate and instead, the fermion correlations must be considered.

The simplest correlation function is the fermion Green function. The Green function is connected to some observables e.g. the spectral function and linear response functions such as conductivity and spin susceptibility. The spectral function in the new phase contains

no quasiparticle poles and the static susceptibilities diverge. Strongly interacting quantum liquids with these properties are called quantum critical [16]. The linear response functions exhibit universal power-law scaling with respect to the frequency and temperature which cannot be reproduced by the LFL. In particular, the dc resistivity shows anomalous power-law scaling with temperature that is similar to the one found in strange metals [17–19]. Theoretical models describing strange metals [20–22] are usually based on some extensions of the Sachdev-Ye-Kitaev (SYK) model [23] that describes strongly interacting fermions with long range all-to-all interaction whose matrix elements are randomly distributed. In our model we do not require any random or even long-range interaction. The quantum criticality in our model emerges due to the resonant many-body exchange interaction between electrons that belong to different Fermi surfaces. Thus, our model might be also important for resolving the mystery of strange metals.

**Fermi surface resonance.** In our study we consider a Fermi gas with multiple non-degenerate Fermi surfaces. This can be experimentally realized in semiconductor heterostructures [24]. Semiconductor heterostructures consist of the thin semiconductor layers. The contact potential between the layers confines electrons or holes within one layer. This leads to quantized energy subbands corresponding to different confined modes. Filling multiple subbands results in multiple Fermi surfaces, see Fig. 1. Generally, the Fermi surfaces are degenerate due to spin. The spin degeneracy can be lifted by an applied magnetic field or by spin-orbit interaction [25]. The spin-orbit interaction can be precisely tuned by electric gates [26]. We assume that  $2N$ ,  $N \geq 2$ , of the non-degenerate Fermi surfaces can be tuned close to the Fermi surface resonance (FSR)

$$\mathcal{K} = 0 \quad (2)$$

where

$$\mathcal{K} = k_1 + \dots + k_{N+\sigma} - k_{N+\sigma+1} - \dots - k_{2N} \quad (3)$$

Here,  $\sigma \in \{0, 1, \dots, N-1\}$ ,  $k_a > 0$  are the corresponding Fermi momenta. Not all Fermi surfaces are required to take part in the resonance. The Fermi surfaces are assumed to be spherically symmetric. This is often the case in semiconductor heterostructures because the electron and hole dispersions at small densities are nearly isotropic [27].

Equation 2 can be thought of as a radial nesting of the Fermi surfaces. Generally, nesting implies a one-dimensional character of the scattering between the nested parts of the Fermi surface. This leads to strong enhancement of such scattering which can trigger an instability. Celebrated examples of instabilities driven by nesting are the charge and spin density orders [28, 29]. The radial nesting is also known to result in strongly interacting electron states such as fractional topological insulators with a gap [30, 31]. In our study we show that

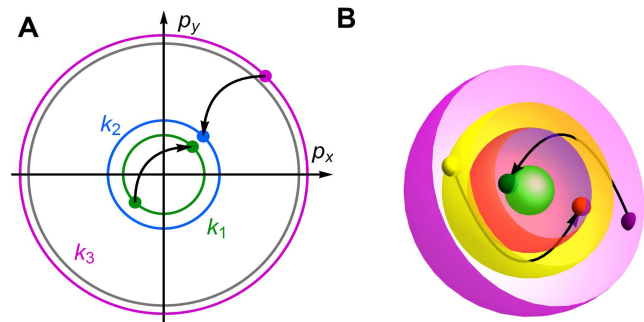


FIG. 1. **Examples of the FSR.** Some of the elementary resonant processes (not all of them) are shown by the arrows. (A) The simplest example of FSR can be realized in semiconductor heterostructures with two filled subbands. The spin degeneracy of the subbands is lifted by the applied magnetic field. The resonant Fermi surfaces are indicated by color. The gray Fermi surface is off resonance. (B) 3D example of the FSR. Only the resonant Fermi surfaces are shown.

the radial nesting of the Fermi surfaces given by Eq. 2 leads to a gapless quantum critical state.

In the general formulation of the problem we require all  $2N$  non-degenerate Fermi surfaces participating in the resonant  $N \rightarrow N$  scattering (see Eqs. 2, 3) to be different. However, we can soften this and only require that the  $N$  initial states belong to different Fermi surfaces, and similarly for the  $N$  final states; some of the initial states might then have the same Fermi surface index as some of the final states. The example shown in Fig. 1A corresponds to this soft formulation because the green Fermi surface contains initial and final states. The integer  $N$  in the soft formulation corresponds to the  $N$ -particle resonant scattering amplitude, e.g.  $N = 2$  in Fig. 1A.

In order to study the new quantum critical phase experimentally, one has to satisfy the single resonant condition given by Eq. 2. In addition, one has to ensure that the Fermi gas is strongly interacting, i.e.  $r_s \gg 1$ . We argue that semiconductor heterostructures are most promising candidates for the experimental search for such new phases. The simplest example of a semiconductor heterostructure which can host a new exotic quantum critical phase is shown in Fig. 1A that represents the Fermi surfaces of a two-dimensional electron gas with two occupied subbands. Even though the occupation of multiple subbands is experimentally achievable [32, 33], the experimental research of materials with multiple Fermi surfaces is still very limited which partially explains why these new phase has never been detected before. Each subband in Fig. 1A is split by an external magnetic field. Changing the electron density and fine tuning by the magnetic Zeeman splitting we can set the system to the FSR given by the condition

$$2k_1 + k_2 - k_3 = 0 \quad (4)$$

where  $k_a$  are the Fermi momenta of corresponding Fermi surfaces, see Fig. 1A. The gray Fermi surface in Fig. 1A does not participate in the resonant scattering. The

given example corresponds to the  $N = 2$  particle resonant scattering amplitude within the soft formulation of the FSR because the green Fermi surface contains both initial and final states. The FSR results in the strong mixing of three colored bands in Fig. 1A which destroys quasiparticles in the vicinity of the colored Fermi surfaces. The quasiparticles in the vicinity of the off-resonant gray Fermi surface survive. The new phase in this example has separate Fermi liquid and non-Fermi-liquid components. The latter is established at the resonance given by Eq. 4 and can be experimentally identified from the power-law frequency tail of the spectral function, the anomalous temperature dependence of the dc resistivity, and the divergent static susceptibilities. In Fig. 1B we also provide an example of the strong version of FSR with  $2N = 4$  different Fermi surfaces in three spatial dimensions.

**Effective Hamiltonian.** Now we proceed to the general case of the FSR. Here we assume that all  $2N$  fields participating in the resonance are different, see Eq. 2. All the results that we obtain in this paper also apply to the soft version of the FSR where some initial states might have the same Fermi surface index as some final states, see Fig. 1A. The FSR results in a dramatic change of the ground state because it favors resonant many-body exchange scattering. The FSR is applied to  $2N$  different non-degenerate Fermi surfaces, so we consider an  $N \rightarrow N$  scattering amplitude which is multilinear with respect to each fermion field. As the FSR condition says nothing about initial and final states, we have to sum over all possible choices of  $N$  initial and  $N$  final states out of overall  $2N$  fields corresponding to the  $2N$  Fermi surfaces, yielding

$$V(R) = \sum_{\{j\}} \lambda_j \Psi_{j_1}^\dagger(R) \dots \Psi_{j_N}^\dagger(R) \Psi_{j_{N+1}}(R) \dots \Psi_{j_{2N}}(R) \quad (5)$$

where  $V(R)$  is the effective Hamiltonian,  $R = (t, \mathbf{r})$ ,  $\mathbf{r}$  is a  $D$ -dimensional position vector,  $t$  is time,  $j$  is a permutation of indices  $\{1, \dots, 2N\}$ ,  $\Psi_a(R)$  is the fermion field operator corresponding to the  $a^{\text{th}}$  Fermi surface, and  $\lambda_j$  are the coupling constants. We sum over all non-equivalent permutations corresponding to  $C_{2N}^N = (2N)!/(N!)^2$  different choices of initial and final states. For conjugate terms the corresponding  $\lambda_j$  is complex conjugate in order to ensure hermiticity of  $V(R)$ . The effective Hamiltonian  $V(R)$  is of exchange form as it mixes together all  $2N$  fermion fields corresponding to the  $2N$  Fermi surfaces participating in the resonance. Similar in spirit is the effective Hamiltonian approach widely used in condensed matter physics, in particular, in the weakly coupled wire approach where  $N$ -electron effective inter-wire interactions are constructed [34, 35].

In case of the soft formulation the effective Hamiltonian has the same form as Eq. 5. The only difference is that the terms containing the square of field operators vanish due to the Fermi statistics. This is consistent with our requirement that all  $N$  initial states as well as all  $N$  final states belong to  $N$  different Fermi surfaces.

The effective Hamiltonian, see Eq. 5, can be constructed using perturbation theory with respect to the two-particle Coulomb interaction  $v_C$ . The first contribution to  $V(R)$  comes from the tree diagrams in the  $(N - 1)^{\text{th}}$  order in  $v_C$

$$V(R) \propto \Lambda = \frac{v_C^{N-1}}{E_F^{N-2}} = E_F r_s^{N-1} \quad (6)$$

where  $\Lambda$  is the characteristic energy scale of  $V(R)$ ,  $E_F$  the Fermi energy, and  $r_s$  the interaction parameter given by Eq. 1. The power of  $v_C$  corresponds to the order of perturbation theory, the power of  $1/E_F$  corresponds to the number of fermion propagators in the tree diagrams. Notice that the strongly interacting regime  $r_s \gg 1$  also corresponds to  $\Lambda \gg E_F$ . Each of the tree diagrams can be envisioned as a sequence of  $N - 1$  Coulomb exchange scattering events. As all  $2N$  fermions are different, the momentum transfers during the exchange are all in order of the average Fermi momentum  $k_F$ . We are interested in the long range correlations at  $r \gg 1/k_F$ . For such long range correlations the  $N \rightarrow N$  scattering that occurs on the scale of the Fermi wavelength  $\sim 1/k_F$  is effectively local, justifying the locality of  $V(R)$ . All the matrix elements that appear in the tree diagrams for  $V(R)$  are hidden in the coupling constants  $\lambda_j$ . Higher order diagrams for  $V(R)$  only renormalize the coupling constants  $\lambda_j$ . Due to symmetries of specific Hamiltonians some of the coupling constants  $\lambda_j$  might be equal to zero. However, this fact is not important for the further analysis if there are at least some non-zero  $\lambda_j$ .

We argue that  $V(R)$  is the most important scattering amplitude close to the FSR, see Eq. 2. All other terms in the many-body scattering amplitudes are either insensitive to the FSR or contain rapidly oscillating terms on the scale of Fermi wavelength. Here we work within the assumption that at arbitrary filling electrons or holes in semiconductors form the LFL. This means that the interaction which is not sensitive to the FSR cannot significantly change the physics. Interactions that contain oscillating terms can be averaged to zero on large scales  $r \gg 1/k_F$ . This allows one to include such interactions as irrelevant corrections renormalizing the LFL parameters.

The effective Hamiltonian  $V(R)$  is very sensitive to the FSR condition given by Eq. 2. We show in the Supplementary Material (SM) that  $V(R)$  leads to the effective interaction

$$\mathcal{D}(x) \propto \frac{e^{-i\mathcal{K}x}}{|x|^{2\nu}} \quad (7)$$

where  $x$  is the extended radial coordinate  $r$ ,  $\mathcal{K}$  is given by Eq. 3, and

$$\nu = \frac{1}{2}(N - 1)(D - 1) \quad (8)$$

where  $D$  is the spatial dimension. The case  $D = 1$  is special, we discuss it in more detail in the SM. Away from the FSR the effective interaction  $\mathcal{D}(x)$  oscillates on the scale  $1/|\mathcal{K}|$ . Thus, only the fluctuations on scales

$|x| \ll 1/|\mathcal{K}|$  are important, the fluctuations on the large scale  $|x| \gg 1/|\mathcal{K}|$  are averaged out due to the oscillating exponent in Eq. 7. Thus, if  $\mathcal{K} \neq 0$  the ground state is the LFL at the large scale  $|x| \gg 1/|\mathcal{K}|$ . However, exactly at the FSR  $\mathcal{K} = 0$  the effective short-range Hamiltonian  $V(R)$  leads to the quasi long-range non-oscillatory effective interaction  $\mathcal{D}(x)$  that is responsible for the LFL breakdown in the infrared limit.

**Spectral density.** In order to study the physical properties of the new phase, we calculate the fermion Green function. For arbitrary parameters this task is very hard. However, at the FSR, see Eq. 2, and in the limit of infinite coupling  $\Lambda/E_F \rightarrow \infty$ , see Eq. 6, the problem can be solved exactly. The infinite coupling is the extreme of the more physical strongly interacting regime  $\Lambda \gg E_F$ , which is guaranteed if  $r_s \gg 1$ . At the FSR and in the infinite coupling limit one can separate the frequency and momentum dependence in the fermion Green function  $G_a(\omega_a, \delta p_a)$ , where  $a$  is the Fermi surface index, and  $\delta p_a = p_a - k_a \ll k_a$  the difference between the momentum  $p_a$  and the Fermi momentum  $k_a$

$$G_a(\omega_a, \delta p_a) \propto \omega_a^\alpha |\delta p_a|^\beta, \quad \text{Im}(\omega_a) > 0 \quad (9)$$

$$\alpha = \frac{1}{N} - 1, \quad \beta = \frac{1-\nu}{N} - 1 \quad (10)$$

where  $\nu$  is given by Eq. 8. Here we suppressed the proportionality coefficient. The derivation of the Green function is given in the SM. The Green function, see Eq. 9, as a function of the complex frequency  $\omega_a$  is analytic in the upper half-plane  $\text{Im}(\omega_a) > 0$ , where  $\text{Im}$  stands for the imaginary part.

The key feature of the LFL is the Landau quasiparticles that appear as sharply defined Lorentzian resonances in the electron spectral function  $\mathcal{A}(\omega, \delta p) = -\text{Im}(G(\omega + i0, \delta p))$ ,  $+i0$  stands for the retarded Green function, and  $\omega$  is the real frequency [15]. The peak position  $\omega = \varepsilon(\delta p)$  defines the quasiparticle spectrum  $\varepsilon(\delta p)$ . However, the electron spectral function corresponding to the Green function given by Eq. 9 does not contain any sharply defined Lorentzian peak and instead is given by

$$\mathcal{A}_a(\omega_a, \delta p_a) \propto |\omega_a|^\alpha |\delta p_a|^\beta \quad (11)$$

where the critical exponents  $\alpha$  and  $\beta$  are given in Eq. 10. Thus, the spectral function  $\mathcal{A}_a(\omega_a, \delta p_a)$  features a power-law tail with a branch cut singularity at  $\omega_a \rightarrow 0$ . This behavior of the spectral function explicitly shows no Landau quasiparticles and, thus, the breakdown of the LFL. The universal power-law scaling is a clear signature of the quantum criticality. Measuring the spectral function, see Eq. 11, near the FSR can experimentally indicate the proximity to the quantum critical state.

**Stability of the quantum critical point.** In order to find the electron Green function at the FSR, see Eq. 9, we used the infinite interaction limit  $\Lambda/E_F \rightarrow \infty$ , for  $\Lambda$  see Eq. 6. In particular, this allowed us to focus

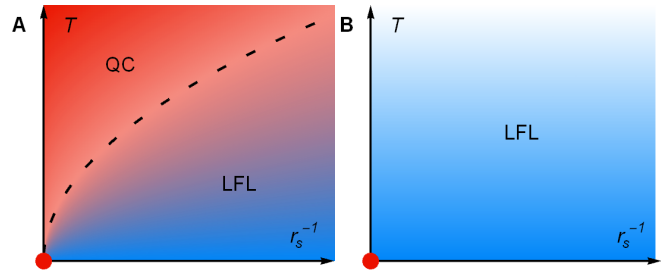


FIG. 2. **Temperature vs.  $r_s^{-1}$  phase diagram at the FSR  $\mathcal{K} = 0$ .** The infinite interaction  $r_s = \infty$  quantum critical point is indicated by the red dot. (A)  $\zeta > 0$ : the quantum criticality is stabilized at finite temperatures  $T \gg T^*$ . The crossover from the QC to the LFL phase is indicated by the dashed line given by Eq. 12. (B)  $\zeta < 0$ : The infinite interaction quantum critical point (red dot) is isolated. Quantum criticality is unstable at any finite interaction parameter  $r_s < \infty$  and any finite temperature  $T$ .

on the effective Hamiltonian  $V(R)$  without taking into account the single-particle Hamiltonian. In real systems the interaction is always finite, therefore we have to check whether our results are stable against the single-particle terms. To do this, we apply the scaling analysis. The details are provided in the SM. Here we just present the results.

We find that at zero temperature the infinite interaction limit is unstable. This means that at any finite interaction  $\Lambda$  the single-particle terms dominate once we are sufficiently close to the Fermi surface, i.e. the LFL is restored in the infrared limit. However, we show that at finite temperatures  $T \gg T^*$  the quantum criticality is stabilized

$$T^* = E_F \left( \frac{E_F}{\Lambda} \right)^\zeta = \frac{E_F}{r_s^{(N-1)\zeta}}, \quad \zeta = \frac{2-\nu}{N-2+\nu} \quad (12)$$

where  $\nu$  is given by Eq. 8,  $r_s \gg 1$  is the interaction parameter, see Eq. 1. This corresponds to the crossover between the quantum critical state and the LFL which is illustrated in Fig. 2. The quantum critical point corresponding to  $r_s \rightarrow \infty$ ,  $T \rightarrow 0$  is indicated by the red dot. This quantum critical point is stable if  $T^* \rightarrow 0$  at  $r_s \rightarrow \infty$ , which is only possible if  $\zeta > 0$ , see Eq. 12. This situation is illustrated in Fig. 2A. In case  $\zeta < 0$  the quantum critical point corresponding to the infinite coupling  $r_s \rightarrow \infty$  is isolated, i.e. the LFL is restored in the infrared limit at any finite interaction strength and any temperature, see Fig. 2B. The case  $\zeta = 0$  is marginal and additional analysis is required. The condition  $\zeta > 0$  at which the quantum criticality survives at finite interaction and finite temperature puts the following constraint

$$N < \frac{D+3}{D-1} \quad (13)$$

The equality  $N = (D+3)/(D-1)$  corresponds to the marginal case  $\zeta = 0$ . For example, in two dimensions the quantum critical regime is possible for  $N \in \{2, 3, 4\}$ , the case  $N = 5$  is marginal. The quantum criticality in three

dimensions is only stable for  $N = 2$ , the case  $N = 3$  is marginal.

Here we have shown that the quantum criticality in higher spatial dimensions  $D > 1$  survives at finite temperatures  $T \gg T^*$ , where  $T^*$  is given by Eq. 12, and at small enough  $N$ , see Eq. 13. There is also an upper bound for the temperature that comes from the sharpness of the Fermi surfaces. In realistic examples, e.g. see Fig. 1A, some Fermi surfaces participating in the FSR are split e.g. by spin-orbit interaction or by an external magnetic field where this splitting is small relative to the subband splitting in the heterostructure. This puts an upper bound for the temperature  $\Delta \gg T$ , where  $\Delta$  stands for the minimal splitting between the Fermi surfaces e.g. spin-orbit gap or Zeeman splitting. Thus, the quantum critical regime corresponds to the temperature window  $\Delta \gg T \gg T^*$ . In addition,  $N$  has to satisfy Eq. 13.

**Static resistivity.** The static or dc resistivity  $\rho_{dc}$  is one of the easiest characteristics that can be measured experimentally. At small temperatures  $T \ll T^*$ , see Eq. 12, the LFL is restored in the infrared, so the dc resistivity is quadratic in temperature  $\rho_{dc} \propto T^2$  [14]. At higher temperatures  $T \gg T^*$  the quantum criticality is established which strongly affects the temperature dependence of the dc resistivity. Here we imply that  $N$  satisfies Eq. 13.

In general, not all Fermi surfaces participate in the resonance, see e.g. the gray Fermi surface in Fig. 1A. Therefore, even at  $T \gg T^*$  the dc conductivity  $\sigma_{dc} = 1/\rho_{dc}$  contains the LFL contribution  $\sigma_{dc}^{LFL}$  from the off-resonant Fermi surfaces and the quantum critical contribution  $\sigma_{dc}^{QC}$  from the resonant Fermi surfaces

$$\sigma_{dc} = \sigma_{dc}^{LFL} + \sigma_{dc}^{QC} \quad (14)$$

The LFL contribution has the temperature scaling  $\sigma_{dc}^{LFL} \propto 1/T^2$  [14]. The quantum critical contribution to the dc conductivity can be represented with the help of the spectral function given by Eq. 11, see e.g. Ref. [20]

$$\sigma_{dc}^{QC} \propto \frac{1}{T} \sum_{a=1}^{2N} v_a^2 \int \frac{d\mathbf{p}_a d\omega_a}{\cosh^2(\omega_a/2T)} A_a(\omega_a, \delta p_a)^2 \quad (15)$$

where  $T \gg T^*$  is the temperature and  $v_a$  the Fermi velocity near the  $a^{\text{th}}$  Fermi surface. The numerical proportionality coefficient is suppressed for brevity. The vertex correction in Eq. 15 is neglected. In the SM we show that the vertex correction does not affect the temperature scaling of  $\sigma_{dc}^{QC}$ . Due to the separation of frequency and momentum dependence in the spectral function, see Eq. 11, the momentum dependent part does not affect the temperature dependence of  $\sigma_{dc}^{QC}$ . The anomalous power-law dependence of  $\sigma_{dc}^{QC}$  on  $T$  can then be derived from the dimensional analysis of Eq. 15

$$\sigma_{dc}^{QC}(T) \propto T^{-\eta}, \quad \eta = 2 - \frac{2}{N} \quad (16)$$

This scaling holds at high temperatures  $T \gg T^*$ . At  $N = 2$  the frequency integral in Eq. 15 is logarithmically divergent that results in the logarithmic correction

$\sigma_{dc}^{QC} \propto T^{-1} \ln(T/T^*)$  at  $T \gg T^*$ . At small temperatures  $T \ll T^*$  the LFL is restored, so  $\sigma_{dc}^{LFL} \sim \sigma_{dc}^{QC} \propto 1/T^2$  at  $T \ll T^*$ . Thus, at  $T \sim T^*$  the two contributions  $\sigma_{dc}^{LFL}$  and  $\sigma_{dc}^{QC}$  are of the same order of magnitude. As  $\eta < 2$ , see Eq. 16,  $\sigma_{dc}^{QC}$  decreases with temperature at  $T \gg T^*$  parametrically slower than  $\sigma_{dc}^{LFL}$ . Thus, at high temperatures  $T \gg T^*$  the quantum critical contribution to the conductivity dominates over the LFL contribution which corresponds to the following scaling of the dc resistivity

$$\rho_{dc} \propto \begin{cases} T^2, & T \ll T^* \\ T^\eta, & T \gg T^* \end{cases} \quad (17)$$

At  $N = 2$  and  $T \gg T^*$  there is the logarithmic prefactor, so  $\rho_{dc} \propto T/\ln(T/T^*)$ . Thus, the temperature dependence of the dc resistivity can be used as an experimental indicator of the quantum criticality. Of course, the temperature  $T$  has still to be much smaller than any splitting between the Fermi surfaces participating in the resonance.

The case of  $N = 2$  is particularly interesting. In this case the dc resistivity is nearly linear in temperature  $\rho_{dc} \propto T/\ln(T/T^*)$  as soon as  $T \gg T^*$ . This is the characteristic feature of strange metals which have been observed experimentally in cuprates [17, 18] and heavy fermion metals [19]. Current theories of strange metals [20–22] are based on the SYK model [23] that requires long-range interaction and random distribution of the interaction matrix elements. In our model the effective interaction is short range, see Eq. 5. Moreover, there is no randomness involved in the problem. Therefore, the new physical mechanism of the quantum criticality based on the resonant many-body exchange scattering that we propose in our study might play an important role in understanding the nature of strange metals.

**Linear response functions.** Other linear response functions also demonstrate the anomalous power-law behavior with respect to temperature or frequency. Here we provide an example of the charge susceptibilities

$$\chi^{ab}(\omega, q) = \int \frac{d\mathbf{w} d\mathbf{p}}{(2\pi)^{D+1}} G_a(\mathbf{w}, \mathbf{p}) G_b(\mathbf{w} + \omega, \mathbf{p} + \mathbf{q}) \quad (18)$$

where  $a$  and  $b$  are the Fermi surface indices. In the SM we show that the scaling properties are the same for all linear response functions. Moreover, we also show in the SM that the vertex correction which is neglected in Eq. 18 does not affect the scaling. Let us first analyze Eq. 18 at  $T \rightarrow 0$  and  $r_s \rightarrow \infty$  which corresponds to the quantum critical point, see Fig. 2. At small  $q$  and  $\omega$  the zero temperature susceptibilities corresponding to  $a^{\text{th}}$  Fermi surface (i.e.  $b = a$  in Eq. 18) diverge

$$\chi^{aa}(\omega, q) \propto q^{(D+1)\alpha+1} |\omega|^\xi, \quad \xi = \frac{2}{N} - 1, \quad (19)$$

where  $\alpha$  is given by Eq. 10. In case if  $N = 2$ , we get  $\xi = 0$  and the frequency divergence of the susceptibility is logarithmic  $|\omega|^\xi \rightarrow \ln|\omega|$ . Equation 19 shows that the static susceptibility  $\chi^{aa}(0, 0)$  at zero temperature  $T = 0$

diverges. This is the defining property of a quantum critical state [15]. However, at any finite interaction  $r_s < \infty$  the quantum critical regime corresponds to finite temperatures  $T \gg T^*$ , see Fig. 2A. This results in the anomalous temperature dependence of the static susceptibility

$$\chi^{aa}(0, q) \propto q^{(D+1)\alpha+1} T^\xi, T \gg T^* \quad (20)$$

for  $\xi$  see Eq. 19. At  $N = 2$  the critical exponent  $\xi$  vanishes, so the temperature dependence becomes logarithmic  $\chi^{aa}(0, q) \propto q^{(D+1)\alpha+1} \ln T$ . The divergence at  $q \rightarrow 0$  holds even at finite temperature. This is due to the separation of frequency and momentum dependence in the Green function, see Eq. 9. Thus, the divergent static susceptibilities, see Eq. 20, at  $T \gg T^*$ , could be another indicator of the quantum criticality that can be accessed experimentally [36].

Apart from the divergence at small  $q$  and  $\omega$ , the susceptibilities  $\chi^{ab}(\omega, q)$  have a non-analytic singularity at  $q \rightarrow q_{ab}^\pm = |k_a \pm k_b|$  which is called the Kohn anomaly [37], where  $k_a, k_b$  are the corresponding Fermi momenta. In case of  $a = b$ , the Kohn anomaly corresponds to  $q = 2k_a$ . In the SM we show that the vertex correction does not affect the critical exponents, so we can use Eq. 18 to derive the Kohn anomaly

$$\chi^{ab}(\omega, q \approx q_{ab}^\pm) \propto |\omega|^\xi |q - q_{ab}^\pm|^{\frac{D+1}{2}\xi} \quad (21)$$

where  $\xi$  is given in Eq. 19. We assume  $r_s \rightarrow \infty, T \rightarrow 0$  in Eq. 21. This results in power-law singularities with respect to both  $\omega$  and  $q - q_{ab}^\pm$  if  $N \geq 3$ . For  $N = 2$ , the Kohn anomaly results in a logarithmic singularity  $\chi^{ab}(\omega, q \approx q_{ab}^\pm) \propto \ln |\omega| \ln |q - q_{ab}^\pm|$ . At finite interaction  $r_s < \infty$  the quantum critical regime corresponds to finite temperatures  $T \gg T^*$ , so the static Kohn anomaly acquires anomalous temperature dependence while the singularity at  $q = q_{ab}^\pm$  remains sharp

$$\chi^{ab}(0, q \approx q_{ab}^\pm) \propto T^\xi |q - q_{ab}^\pm|^{\frac{D+1}{2}\xi} \quad (22)$$

For  $N = 2$  the singularity is logarithmic  $\chi^{ab}(0, q \approx q_{ab}^\pm) \propto \ln T \ln |q - q_{ab}^\pm|$ . The sharp singularity of the static susceptibility at  $q = q_{ab}^\pm$  is due to the separation of frequency and momentum dependence in the Green function, see Eq. 9.

The divergent Kohn anomalies and one-dimensional character of the radially nested scattering resonance may lead to the spatially inhomogeneous orders. For example, coupling to phonons may result in the charge density order due to the Peierls instability [38]. Another example comes from the Ruderman-Kittel-Kasuya-Yoshida (RKKY) exchange interaction between magnetic impurities that is mediated by itinerant fermions [39]. Magnetic helical order may be established if the spin susceptibility of the itinerant fermions has a divergent Kohn anomaly [40, 41].

**Conclusions.** In our study we theoretically discovered a novel physical state of strongly interacting fermions which can be realized in materials with multiple

Fermi surfaces that are subject to a special resonant condition given by Eq. 2. This phase can be experimentally identified by the spectral function showing no Landau quasiparticles close to the Fermi surface, by the anomalous power-law temperature dependence of the dc resistivity, and by the divergent static susceptibilities. We believe that the new exotic phase that we predict in this paper can be found for instance in semiconductor heterostructures because of the large interaction parameter  $r_s \gg 1$ . Moreover, the high quality and tunability of the semiconductor devices makes it possible to tune the system to the FSR, see Eq. 2, which is required for establishing the new quantum critical state.

**ACKNOWLEDGEMENTS.** We acknowledge support by the Georg H. Endress foundation, the Swiss National Science Foundation, and NCCR QSIT. This project received funding from the European Union's Horizon 2020 research and innovation program (ERC Starting Grant, grant agreement No 757725).

## SUPPLEMENTARY MATERIAL

In the Supplementary Material (SM) we provide technical details that justify the physical results that we discuss in the main text. Here we derive the fermion Green function within the self-consistent Born approximation (SCBA) with the effective interaction given by Eq. 5 in the main text. We consider the strong coupling regime, so the single-particle spectral part is suppressed. The emergent conformal symmetry of the SCBA Dyson equation signals the renormalization group (RG) fixed point of the effective Hamiltonian given by Eq. 5 in the main text. At the RG fixed point the interaction coupling constant renders to the fixed value in the infrared limit. Thus, the interaction vertex correction just redefines the bare coupling constant without affecting the conformal scaling dimensions. This makes the SCBA exact in the infrared limit. We also check the stability of our results with respect to the single-particle terms that we dropped during the SCBA. Using the RG arguments, we show that the RG fixed point is only stable at finite temperatures  $T \gg T^*$ ,  $T^*$  is given by Eq. 12 in the main text, and for small enough  $N$ , see Eq. 13 in the main text. Using the conformal symmetry, we calculate the response functions such as the dc conductivity and charge susceptibilities. All these results are derived for spatial dimension  $D > 1$ . We also expect quantum criticality in the one-dimensional case, though it is not exactly clear how to proceed with this problem using the bosonization technique.

**Self-consistent Born approximation.** In this section we calculate the fermion Green function dressed by the effective interaction  $V(R)$ , see Eq. 5 in the main text. Here we assume that the interaction is strong, so it completely destroys quasiparticles close to the Fermi surfaces. The notion of Fermi surfaces is still important though because they define the sector of quantum states that are the most affected by the interaction  $V(R)$ . Such Fermi surfaces without quasiparticles are known as critical Fermi surfaces [21]. In this section we apply the SCBA i.e. we neglect renormalization of the interaction vertex. We also work within the strong coupling regime, so we assume that the Green function close to the Fermi surfaces is entirely defined by its self-energy. This allows us to neglect the single-particle spectral part close to the Fermi surfaces. This does not mean that we completely neglect the single-particle effects because we still rely on the Fermi surface structure. Only the spectral part very close to the Fermi surfaces is suppressed.

Away from the FSR that is defined by Eqs. 2-3 in the main text the ground state of the interacting Fermi gas is the LFL. This means that the system is well described by the long-lived Landau quasiparticles which are represented by the poles of the Green function

$$G_a^{(0)}(\omega_a, \delta p_a) = \frac{Z_a}{\omega_a - v_a \delta p_a} \quad (\text{S1})$$

where the index  $a \in \{1, \dots, 2N\}$  enumerates the Fermi

surfaces,  $\omega_a$  is the frequency that we allow to be complex,  $\delta p_a = p_a - k_a$ , with  $|\delta p_a| \ll k_a$ , is the difference of the momentum  $p_a$  from the Fermi momentum  $k_a$ ,  $v_a$  is the Fermi velocity which is renormalized by irrelevant interactions, and  $1 > Z_a > 0$  is the quasiparticle residue. Throughout this section we assume zero temperature.

Once we are close to the FSR, see Eqs. 2-3 in the main text, the resonant many-body exchange scattering described by the effective Hamiltonian  $V(R)$  kicks in, see Eq. 5 in the main text. In the main text we argued that other scattering amplitudes that are insensitive to the resonant condition  $\mathcal{K} = 0$  are not important as they only contribute to the LFL parameters such as the Fermi velocities  $v_a$  and the quasiparticle residues  $Z_a$ . The contribution of  $V(R)$  has to be treated separately and is included via the self-energy  $\Sigma_a(\omega_a, \delta p_a)$

$$G_a(\omega_a, \delta p_a) = \frac{1}{G_a^{(0)}(\omega_a, \delta p_a)^{-1} - \Sigma_a(\omega_a, \delta p_a)} \quad (\text{S2})$$

where  $G_a^{(0)}(\omega_a, \delta p_a)$  is given by Eq. S1 and contains the contributions from the irrelevant interactions.

The Green function  $G_a(\omega_a, \delta p_a)$  is analytic in the upper half-plane  $\text{Im}(\omega_a) > 0$ ,  $\text{Im}$  stands for the imaginary part. This property is manifested by the spectral representation

$$G_a(\omega_a, \delta p_a) = \int_{-\infty}^{\infty} \frac{dz}{\pi} \frac{\mathcal{A}_a(z, \delta p_a)}{\omega_a - z} \quad (\text{S3})$$

where  $\mathcal{A}_a(\omega_a, \delta p_a) = -\text{Im}[G_a(\omega_a + i0, \delta p_a)] > 0$  is the spectral function. The spectral representation Eq. S3 allows one to get various Green functions. For example, the Matsubara Green function corresponds to pure imaginary frequencies, the retarded (advanced) Green function corresponds to  $\omega_a \rightarrow \omega_a + i0$  ( $\omega_a \rightarrow \omega_a - i0$ ). In what follows we consider the Matsubara Green function. In cases when we need other Green functions, we use the analytical continuation via Eq. S3.

The Feynman diagram for the exact self-energy for  $N = 2$  is presented in Fig. S1A and corresponds to the example shown in Fig. 1B in the main text. Feynman diagrams for general  $N$  can be constructed in a similar fashion. The problem here is the renormalization of the interaction vertex, see black square in Fig. S1A. In this section we omit the interaction vertex renormalization and instead consider the simpler diagram in Fig. S1B. Such approximation is called the self-consistent Born approximation (SCBA). The diagrams of the form in Fig. S1B are also known as ‘‘melon’’ diagrams that appear in various matrix and tensor field theories [42].

Within the SCBA, see Fig. S1B, the self-energy  $\Sigma_1(t, \delta p_1)$  is self-consistently expressed through the Green functions

$$\Sigma_1(t, \delta p_1) = (-1)^{N-1} \sum_{\{\eta\}} |\lambda_\eta|^2 \int \prod_{a=2}^{2N} \frac{d\mathbf{p}_a}{(2\pi)^D} G_a(\eta_a t, \delta p_a) \times \\ (2\pi)^D \delta \left( \mathbf{p}_1 - \sum_{b=2}^{2N} \eta_b \mathbf{p}_b \right) \quad (\text{S4})$$

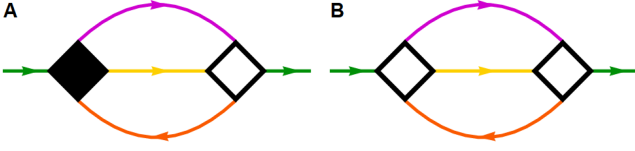


FIG. S1. **Electron self-energy.** (A) Feynman diagram for the exact self-energy for the case  $N = 2$ . Solid lines correspond to the exact Green functions, see Eq. S2. The Fermi surface index  $a \in \{1, 2, 3, 4\}$  is indicated by color and corresponds to the example given in Fig. 1B in the main text. The black (white) square corresponds to the exact (bare) interaction vertex. There are two more contributions to the self-energy that differ by the arrow directions. The Feynman diagrams for general  $N$  can be constructed similarly. (B) The SCBA. The interaction vertex correction is neglected which is shown by two bare vertices (white squares).

where  $\lambda_\eta$  are bare interaction couplings, see Eq. 5 in the main text,  $D$  is the spatial dimension. We consider the self-energy corresponding to the electrons near the 1<sup>st</sup> Fermi surface, the result is similar for other Fermi surface indices. The  $\delta$ -function denotes the momentum conservation. Each  $\eta = (\eta_2, \dots, \eta_{2N})$ ,  $\eta_b = \pm 1$ , corresponds to one of the choices to draw arrows on the Feynman diagram. The charge conservation requires the following constraint

$$\sum_{b=2}^{2N} \eta_b = 1 \quad (\text{S5})$$

This gives overall  $C_{2N-1}^N = (2N-1)!/(N!(N-1)!)$  terms in the sum over  $\eta$ .

The spherical symmetry of the Fermi surfaces makes the Green functions independent of the angular variables. This allows us to perform exact angular integration using the following identities

$$(2\pi)^D \delta\left(\mathbf{p}_1 - \sum_{b=2}^{2N} \eta_b \mathbf{p}_b\right) = \int d\mathbf{r} e^{i\mathbf{r} \cdot \left(\mathbf{p}_1 - \sum_{b=2}^{2N} \eta_b \mathbf{p}_b\right)} \quad (\text{S6})$$

$$\int \frac{d\mathbf{p}_a}{(2\pi)^D} e^{\pm i\mathbf{r} \cdot \mathbf{p}_a} f(\delta p_a) \approx k_a^{D-1} \int_{-\infty}^{\infty} \frac{d\delta p_a}{2\pi} f(\delta p_a) J(rp_a) \quad (\text{S7})$$

$$J(z) = \int \frac{d\Omega_D}{(2\pi)^{D-1}} e^{iz \cos \theta} \approx \frac{e^{iz}}{(2\pi iz)^{\frac{D-1}{2}}} + \frac{e^{-iz}}{(-2\pi iz)^{\frac{D-1}{2}}} \quad (\text{S8})$$

where in Eq. S7 we substituted  $p_a^{D-1} \rightarrow k_a^{D-1}$  as  $|\delta p_a| = |p_a - k_a| \ll k_a$ ,  $k_a$  is the corresponding Fermi momentum,  $f(\delta p_a)$  is an arbitrary function,  $d\Omega_D$  is the volume element of the  $D$ -dimensional solid angle. In Eq. S8 we provided the asymptotic behavior of  $J(z)$  at  $|z| \gg 1$ . Using these relations, we can represent the self-energy in the following form

$$\Sigma_1(t, \delta p_1) = (-1)^{N-1} \sum_{\{\eta\}} |\lambda_\eta|^2 \int \prod_{a=2}^{2N} \frac{d\delta p_a}{2\pi} G_a(\eta_a t, \delta p_a) \times \mathcal{D}(\delta p_1, \dots, \delta p_{2N}) \quad (\text{S9})$$

$$\mathcal{D}(\delta p_1, \dots, \delta p_{2N}) = \left(\frac{2\pi}{k_1}\right)^{D-1} \int_0^\infty dr r^{D-1} \prod_{a=1}^{2N} k_a^{D-1} J(rp_a) \quad (\text{S10})$$

The function  $\mathcal{D}(\delta p_1, \dots, \delta p_{2N})$  is well defined, with the integral over  $r$  being convergent. We are interested in the long range correlations occupying the sector  $k_a r \gg 1$ , so we can use the asymptotic expansion of  $J(z)$ , see Eq. S8. As we clearly see, at arbitrary Fermi surfaces the function  $\mathcal{D}(\delta p_1, \dots, \delta p_{2N})$  is strongly oscillating on the scale of Fermi wavelength. However, once the FSR condition  $\mathcal{K} = 0$  is approached, the product of  $J$ -functions in Eq. S10 contains two non-oscillatory terms. Therefore, close to the FSR we suppress all the oscillatory terms and only keep the resonant slowly varying ones

$$\mathcal{D}(\delta p_1, \dots, \delta p_{2N}) \approx 2c_1 \text{Re} \left( \int_0^\infty \frac{dr}{r^{2\nu}} i^{\sigma(D-1)} e^{-ir\mathcal{K}} e^{-ir\delta p} \right) \quad (\text{S11})$$

$$c_1 = \left(\frac{k_F}{k_1}\right)^{D-1} \left(\frac{k_F}{2\pi}\right)^{2\nu} \quad (\text{S12})$$

where  $\sigma$  is defined in Eq. 3 in the main text,  $\nu$  is given by Eq. 8 in the main text,  $k_F = (k_1 \dots k_{2N})^{1/2N}$  is the average Fermi momentum,  $\mathcal{K} \ll k_a$  is the detuning from the FSR,  $\text{Re}$  stands for the real part, and  $\delta p$  is the following combination of the momenta

$$\delta p = \delta p_1 + \dots + \delta p_{N+\sigma} - \dots - \delta p_{2N} \quad (\text{S13})$$

Thus, close to the resonance the function  $\mathcal{D}(\delta p_1, \dots, \delta p_{2N})$  becomes a function of  $\delta p$  only. As we consider spatial dimensions  $D > 1$ , the integral over  $r$  in Eq. S11 is divergent if  $r \rightarrow 0$ . This is due to the fact that the asymptotics of  $J(z)$  that we used there is not applicable at small arguments. Thus, the integral over  $r$  in Eq. S11 has to be cut at  $r \sim 1/k_F$ . This problem can be resolved by taking the Fourier transform of  $\mathcal{D}(\delta p)$

$$\mathcal{D}(x) = \int_{-\infty}^{\infty} \frac{d\delta p}{2\pi} e^{i\delta p x} \frac{\mathcal{D}(\delta p)}{c_1} = \frac{e^{-i\mathcal{K}x}}{|x|^{2\nu}} [i \text{sign}(x)]^{\sigma(D-1)} \quad (\text{S14})$$

Here we divided by the constant  $c_1$  in order to make  $\mathcal{D}(x)$  independent of the Fermi surface index. The divergent part of  $\mathcal{D}(\delta p)$  transforms into a short range singularity of  $\mathcal{D}(x)$  at  $x \rightarrow 0$  which has to be cut at  $|x| \sim 1/k_F$ ,  $k_F$  is the average Fermi momentum. We call the coordinate  $x$  the extended radial coordinate because it is conjugate to the shifted radial momentum  $\delta p$ . Equation S14 clearly supports the argument that the long-range correlations are only possible at  $\mathcal{K} = 0$ , see the main text. If  $\mathcal{K} \neq 0$ , then the fluctuations at  $|x| \gg 1/|\mathcal{K}|$  are not important due to the oscillating exponent, and thus  $1/|\mathcal{K}|$  defines the finite range of the interaction.

After integrating out the angular variables, we effectively reduced the spatial dimension from  $D$  to one. The dimensional reduction clearly demonstrated that the SCBA is dominated by the s-wave scattering that supports the radially aligned FSR given by Eqs. 2-3 in the

main text. The dimensional reduction brought us the effective interaction  $\mathcal{D}(x)$  which becomes quasi-long-range at the FSR when  $\mathcal{K} = 0$ , see Eq. S14. This is the only difference from a truly one-dimensional problem for which  $\mathcal{D}(x) = 1$  at  $\mathcal{K} = 0$ . The self-energy in the  $(t, x)$  representation is especially simple

$$\Sigma_1(t, x) = (-1)^{N-1} c_1 \sum_{\{\eta\}} |\lambda_\eta|^2 \prod_{a=2}^{2N} G_a(\eta_a t, \pm x) \mathcal{D}(x) \quad (\text{S15})$$

where we take  $-x$  for  $a \in \{2, \dots, N + \sigma\}$  and  $+x$  for the rest. The signs of  $x$  are in correspondence with Eq. S13. Notice that signs of time  $t$  and the effective coordinate  $x$  in the arguments of the Green functions in Eq. S15 are somewhat uncorrelated. This can be resolved by introducing left and right Green functions. And in the truly one-dimensional case this is the route to take. However, in higher dimensions  $D > 1$  the effective interaction  $\mathcal{D}(x)$  is non-trivial which breaks the equivalence between time and space coordinates. As we see further this results in separate temporal and spatial dynamics.

In the strong coupling limit we can suppress the single-particle terms such that the Green function, see Eq. S2, is determined entirely by its self-energy

$$G_a(\omega_a, \delta p_a) \approx -\frac{1}{\Sigma_a(\omega_a, \delta p_a)} \quad (\text{S16})$$

We emphasize that the Fermi surface structure was used to perform the dimensional reduction and plays a crucial role in the FSR, so we do not entirely neglect the single-particle effects. However, we argue that the spectral part close to the Fermi surfaces can be neglected compared to the interaction contribution. Far from the Fermi surfaces there is no resonant condition and the quasiparticle picture holds. Therefore, the Fermi surfaces define the quantum states that are the most affected by the interaction. These quantum states represent the infrared sector that we are interested in the most. In the  $(t, x)$  representation Eq. S16 takes the integral form

$$\delta(t)\delta(x) = - \int dt' dx' G_a(t-t', x-x') \Sigma_a(t', x') \quad (\text{S17})$$

Substituting Eq. S15 into Eq. S17 results in the integral Dyson equation for the Green function in the strong coupling limit

$$\delta(t)\delta(x) = (-1)^N c_1 \int dt' dx' G_1(t-t', x-x') \times \sum_{\{\eta\}} |\lambda_\eta|^2 \prod_{a=2}^{2N} G_a(\eta_a t', \pm x') \mathcal{D}(x') \quad (\text{S18})$$

Equation S18 is the SCBA for the Green function in the limit of strong interaction.

At the FSR the effective interaction  $\mathcal{D}(x)$  is quasi-long-range, i.e. it looks the same at all scales. Therefore, Eq. S18 does not contain any physical energy or length scale. This observation suggests that the Green functions are also universal scaling functions. As all  $2N$  Green functions are in the product in Eq. S18, we expect the

same critical exponents for all of them regardless of the index  $a$ . The effective interaction  $\mathcal{D}(x)$  results in different scaling with time and coordinate. Simple dimensional analysis of Eq. S18 yields

$$G_a(t, x) \propto \frac{1}{t^{2h}} \frac{1}{x^{2l}}, \quad h = \frac{1}{2N}, \quad l = \frac{1-\nu}{2N} \quad (\text{S19})$$

where  $\nu$  is given by Eq. 8 in the main text. The critical exponents  $h$  and  $l$  play the role of the conformal dimensions of the fermion fields. As  $\nu > 0$  at  $D > 1$ , the temporal  $h$  and spatial  $l$  conformal dimensions are different which naturally suggests the separation of temporal and spatial dynamics

$$G_a(t, x) = C_a g(t) \gamma(x) \quad (\text{S20})$$

where  $C_a$  is some constant that might be different for different  $a$ . This ansatz is different from the truly one-dimensional case  $D = 1$  in which the temporal and spatial scalings are the same and the separation argument does not apply. Instead, left and right linear combinations of time and coordinate must be used for  $D = 1$ . Thus, our current analysis of Eq. S18 is only applicable for  $D > 1$ . The Dyson equation S18 then separates into a time and a coordinate equation

$$\delta(t) = (-1)^{N-1} \int dt' g(t-t') g(-t')^{N-1} g(t')^N \quad (\text{S21})$$

$$\delta(x) = - \int dx' \gamma(x-x') \gamma(-x')^{N+\sigma-1} \gamma(x')^{N-\sigma} \mathcal{D}(x') \quad (\text{S22})$$

The coefficients  $C_a$  then satisfy the following algebraic equation

$$c_1 \sum_{\{\eta\}} |\lambda_\eta|^2 \prod_{a=1}^{2N} C_a = 1 \quad (\text{S23})$$

We can choose all coefficients  $C_a$  positive, i.e.  $C_a > 0$ . Non-trivial phases can come from solutions for  $g(t)$  and  $\gamma(x)$  which we consider later. All coefficients  $C_a > 0$  are combined in the single product in Eq. S23, so it is not possible to determine them separately without connecting the infrared interaction-dominated limit with the ultraviolet limit far from Fermi surfaces which is given by the LFL. The coefficients  $C_a$  scale with the interaction strength as  $C_a \propto \lambda^{-1/N}$ , where we introduced the combined interaction strength parameter  $\lambda^2 = \sum_{\{\eta\}} |\lambda_\eta|^2$ . This corresponds to the self-energy scaling  $\Sigma_a \propto \lambda^{1/N}$  which justifies the strongly interacting limit  $\lambda \rightarrow \infty$  at which the self-energy correction is dominant over the single-particle spectral part. Apart of the considered interaction scaling, the coefficients  $C_a$  play no role in the infrared physics that we study here, so we can concentrate on the universal functions  $g(t)$  and  $\gamma(x)$ .

Equation S21 is the Dyson equation for the generalized Sachdev-Ye-Kitaev (SYK) model, called the  $q$ -SYK,  $q = 2N$  in our case [23, 43]. The SYK model describes  $(0+1)$ -dimensional strongly correlated fermions with all-to-all interactions whose matrix elements are randomly distributed. Here, quite remarkably, we observe the same

temporal dynamics for our  $(D + 1)$ -dimensional system without having any randomness in our model and for short-range interactions given by the Hamiltonian  $V(R)$ , see Eq. 5 in the main text. The exact Green function  $g(t)$  of the  $q$ -SYK model exhibits the power-law scaling which is correctly captured by Eq. S19.

Here we outline the derivation of the zero-temperature Matsubara Green function  $g(t)$ , following Ref. [43]. The solution can be found with the help of the following ansatz

$$g(t) = \frac{g_1 \mathcal{H}(t) + g_2 \mathcal{H}(-t)}{|t|^{2h}} \quad (\text{S24})$$

where  $g_{1,2}$  are some constants,  $h$  is the temporal conformal dimension,  $\mathcal{H}(t)$  is the Heaviside step function which is 0 at  $t < 0$  and 1 at  $t > 0$ . Taking the Fourier transform of Eq. S21, we get the following equation

$$1 = (-1)^{N-1} g(\omega) \Sigma_g(\omega) \quad (\text{S25})$$

$$g(\omega) = \int_{-\infty}^{\infty} g(t) e^{i\omega t} dt$$

$$= \Gamma(-\alpha) \left( g_1 i^{-\alpha \text{sign}(\omega)} + g_2 i^{\alpha \text{sign}(\omega)} \right) |\omega|^\alpha \quad (\text{S26})$$

$$\Sigma_g(\omega) = \int_{-\infty}^{\infty} g(-t)^{N-1} g(t)^N e^{i\omega t} dt$$

$$= \Gamma(\alpha') (g_1 g_2)^{N-1} \left( g_1 i^{\alpha' \text{sign}(\omega)} + g_2 i^{-\alpha' \text{sign}(\omega)} \right) |\omega|^{-\alpha'} \quad (\text{S27})$$

$$\alpha = 2h - 1, \alpha' = 1 - 2h(2N - 1) \quad (\text{S28})$$

where we introduced the temporal part of self-energy denoted by  $\Sigma_g$ ,  $\Gamma(z)$  is the Euler  $\Gamma$ -function. In order to satisfy Eq. S25, we have to equate  $\alpha$  and  $\alpha'$  which gives the temporal conformal dimension

$$h = \frac{1}{2N}, \alpha = \alpha' = \frac{1}{N} - 1 \quad (\text{S29})$$

This is consistent with simple dimensional analysis of Eq. S21 that is given by Eq. S19. Once this is sorted, Eq. S25 gives the algebraic equation for the constants  $g_{1,2}$

$$(-g_1 g_2)^{N-1} (g_1^2 + g_2^2 + 2g_1 g_2 \cos \pi \alpha) = -\frac{\alpha}{\pi} \sin \pi \alpha \quad (\text{S30})$$

where  $\alpha$  is given by Eq. S29.

Equation S22 differs from Eq. S21 by the factor  $\mathcal{D}(x)$  which plays the role of the propagator of an emergent conformal field, as we will see later. Nevertheless, Eq. S22 can be solved with the help of a similar ansatz

$$\gamma(x) = \frac{\gamma_1 \mathcal{H}(x) + \gamma_2 \mathcal{H}(-x)}{|x|^{2l}} \quad (\text{S31})$$

where  $\gamma_{1,2}$  are some constants,  $l$  is the spatial conformal dimension. Taking the Fourier transform of Eq. S22, we get the following equation

$$1 = -\gamma(\delta p) \Sigma_\gamma(\delta p) \quad (\text{S32})$$

$$\gamma(\delta p) = \int_{-\infty}^{\infty} \gamma(x) e^{-i\delta p x} dx$$

$$= \Gamma(-\beta) \left( \gamma_1 i^{\beta \text{sign}(\delta p)} + \gamma_2 i^{-\beta \text{sign}(\delta p)} \right) |\delta p|^\beta \quad (\text{S33})$$

$$\Sigma_\gamma(\delta p) = \int_{-\infty}^{\infty} \gamma(-x)^{N+\sigma-1} \gamma(x)^{N-\sigma} \mathcal{D}(x) dx = \Gamma(\beta') (\gamma_1 \gamma_2)^{N-\sigma-1} \times$$

$$\left( \gamma_1 \gamma_2^{2\sigma} i^{\sigma(D-1)-\beta' \text{sign}(\delta p)} + \gamma_1^{2\sigma} \gamma_2 i^{-\sigma(D-1)+\beta' \text{sign}(\delta p)} \right) |\delta p|^{-\beta'} \quad (\text{S34})$$

$$\beta = 2l - 1, \beta' = 1 - 2l(2N - 1) - 2\nu \quad (\text{S35})$$

In order to satisfy Eq. S32, we have to set  $\beta$  and  $\beta'$  equal which yields the spatial conformal dimension

$$l = \frac{1-\nu}{2N}, \beta = \beta' = \frac{1-\nu}{N} - 1 = \frac{D+1}{2} \left( \frac{1}{N} - 1 \right) \quad (\text{S36})$$

Of course, this is consistent with the simple dimensional analysis given by Eq. S19. Once the conformal dimension  $l$  is identified, Eq. S32 yields the following algebraic equation for the constants  $\gamma_{1,2}$

$$\left( \gamma_1^{2\sigma+1} \gamma_2 i^{-\sigma(D-1)+2\beta \text{sign}(\delta p)} + \gamma_1 \gamma_2^{2\sigma+1} i^{\sigma(D-1)-2\beta \text{sign}(\delta p)} \right.$$

$$\left. + \gamma_1^{2\sigma} \gamma_2^2 i^{-\sigma(D-1)} + \gamma_1^2 \gamma_2^{2\sigma} i^{\sigma(D-1)} \right) (\gamma_1 \gamma_2)^{N-\sigma-1} = \frac{\beta}{\pi} \sin \pi \beta \quad (\text{S37})$$

Notice that Eq. S37 still depends on the sign of  $\delta p$ . If  $\sigma = 0$ , then the terms in Eq. S37 that contain  $\text{sign}(\delta p)$  can be combined into  $\cos(\pi \beta \text{sign}(\delta p))$  which is independent of the sign of  $\delta p$ . However, if  $\sigma \neq 0$ , we have to put an additional constraint

$$\gamma_1 = e^{i\phi} \gamma_2, \phi = \frac{\pi}{2} (D-1) + \frac{\pi n}{\sigma}, \sigma \neq 0 \quad (\text{S38})$$

where  $n$  is an integer. The phase  $\phi$  can be further simplified

$$\phi = \frac{\pi}{2} r_\phi + \frac{\pi n'}{\sigma}, r_\phi = \sigma(D-1) \bmod 2 \quad (\text{S39})$$

where  $r_\phi \in \{0, 1\}$  is the residue from dividing  $\sigma(D-1)$  by 2,  $n'$  is an integer which is different from  $n$ , see Eq. S38. The resulting equation for  $\gamma_{1,2}$  in case of any  $\sigma$  can be written in the following compact form

$$(\gamma_1 \gamma_2)^{N-1} (\gamma_1^2 + \gamma_2^2 + 2\gamma_1 \gamma_2 \cos \pi \beta) = \mathcal{P}_\sigma \frac{\beta}{\pi} \sin \pi \beta \quad (\text{S40})$$

where  $\beta$  is given by Eq. S36,  $\mathcal{P}_\sigma = 1$  if  $\sigma = 0$  and  $\mathcal{P}_\sigma = e^{i\pi n}$  if  $\sigma \neq 0$  with the integer  $n$  defined in Eq. S38. In case of  $\sigma \neq 0$ , the constants  $\gamma_{1,2}$  are not independent and satisfy Eq. S38.

As we aim to calculate the spectral function, we take the Fourier transform of the Matsubara Green function  $G_a(t, x)$ , see Eqs. S20, S26, S33

$$G_a(i\omega, \delta p) = C_a \left( g_1 i^{-2\alpha \text{sign}(\omega)} + g_2 \right) \times$$

$$\left( \gamma_1 i^{\beta \text{sign}(\delta p)} + \gamma_2 i^{-\beta \text{sign}(\delta p)} \right) |\delta p|^\beta (i\omega)^\alpha \quad (\text{S41})$$

where  $C_a > 0$  is some coefficient which is generally different from the one we introduced in Eq. S20. Using the analytic properties of the Green function, we can analytically continue it for all complex  $\omega$  such that  $\text{Im}(\omega) > 0$

$$G_a(\omega, \delta p) = C_a \left( g_1 e^{-i\pi \alpha} + g_2 \right) \times$$

$$\left( \gamma_1 i^{\beta \text{sign}(\delta p)} + \gamma_2 i^{-\beta \text{sign}(\delta p)} \right) |\delta p|^\beta \omega^\alpha \quad (\text{S42})$$

The retarded Green function corresponds to the choice  $\omega \rightarrow \omega + i0$  for real  $\omega$ . This allows us to find the spectral density as  $\mathcal{A}_a(\omega, \delta p) = -\text{Im}(G_a(\omega + i0, \delta p))$ . Even without knowing the coefficients  $g_{1,2}$ ,  $\gamma_{1,2}$  we can obtain the frequency and momentum scaling of the spectral function

$$\mathcal{A}_a(\omega, \delta p) \propto |\delta p|^\beta |\omega|^\alpha \quad (\text{S43})$$

This readily shows that there are no quasiparticle resonances in the spectral function close to the Fermi surface. Quasiparticles are replaced by the incoherent branch-cut singularity at  $\omega \rightarrow 0$ . We provide this result in the main text.

Here we would like to comment on the particle-hole symmetry which is given by the symmetry condition on the spectral function

$$\mathcal{A}_a(-\omega, -\delta p) = \mathcal{A}_a(\omega, \delta p) \quad (\text{S44})$$

We omitted the single-particle terms here which are particle-hole symmetric close to the Fermi surfaces. The interaction  $V(R)$  together with the self-consistent Dyson equation S18 also respect the particle-hole symmetry. However, it is not obvious that this symmetry can be satisfied by the solution given by Eq. S42 due to dependence on the sign of  $\delta p$ . If  $\sigma = 0$  we can always choose  $\gamma_1 = \gamma_2$  which eliminates the sign of  $\delta p$ . If  $\sigma \neq 0$  we are constrained by Eq. S38. According to Eq. S39, we can choose  $\phi = 0$  if  $\sigma(D - 1)$  is an even integer. This gives  $\gamma_1 = \gamma_2$ , see Eq. S38, so no difference from  $\sigma = 0$  case. In this case the retarded Green function  $G_a^R(\omega, \delta p)$  has the following analytic form

$$G_a^R(\omega, \delta p) = C_a e^{-i\theta} |\delta p|^\beta (\omega + i0)^\alpha, \quad \sigma(D - 1) = 0 \pmod{2} \quad (\text{S45})$$

where we included all positive constants in a new  $C_a > 0$  for brevity, the phase  $\theta$  is defined as follows

$$\theta = -\arg(g_1 e^{-i\pi\alpha} + g_2) \quad (\text{S46})$$

In order to satisfy the particle-hole symmetry given by Eq. S44, one has to choose  $\theta = \pi/2N$  with corresponding spectral density

$$\mathcal{A}_a(\omega, \delta p) = -\text{Im}(G_a^R(\omega, \delta p)) = C_a \sin\left(\frac{\pi}{2N}\right) |\delta p|^\beta |\omega|^\alpha \quad (\text{S47})$$

However, the phase  $\phi$  cannot be completely eliminated if  $\sigma(D - 1)$  is an odd integer. In this case  $\phi$  is equal to  $\pi/2$  modulo  $\pi/\sigma$ , see Eq. S39. This results in the spontaneously broken particle-hole symmetry due to the following identity

$$\gamma_1 i^{\beta \text{sign}(\delta p)} + \gamma_2 i^{-\beta \text{sign}(\delta p)} = 2\gamma_2 e^{i\frac{\phi}{2}} \cos\left(\frac{\pi\beta}{2} + \frac{\phi}{2} \text{sign}(\delta p)\right) \quad (\text{S48})$$

The spectral density in this case is the following

$$\begin{aligned} \mathcal{A}_a(\omega, \delta p) \propto & \sin\left(\theta - \frac{\phi}{2} - \pi\alpha\mathcal{H}(-\omega)\right) \times \\ & \cos\left(\frac{\pi\beta}{2} + \frac{\phi}{2} \text{sign}(\delta p)\right) |\delta p|^\beta |\omega|^\alpha \end{aligned} \quad (\text{S49})$$

where  $\mathcal{H}(x)$  is the Heaviside step function, and  $\alpha$  and  $\beta$  are defined in Eqs. S29, S36. Here we suppressed a positive constant. It is clear that in this case it is not possible

to satisfy the particle-hole symmetry, see Eq. S44. The electron-hole asymmetry can be experimentally identified by the thermopower coefficient, see e.g. Ref. [44]. Here we also notice that the asymmetry is rather strong as it survives in the infrared limit.

**Emergent conformal symmetry.** The homogeneity condition to the Green functions  $g(t, t') = g(t-t')$  and  $\gamma(x, x') = \gamma(x-x')$  is applied in Eqs. S21, S22. Here we analyze these equations written without the homogeneity condition

$$\delta(t-t') = (-1)^{N-1} \int dt'' g(t, t'') g(t'', t')^{N-1} g(t'', t')^N \quad (\text{S50})$$

$$\delta(x-x') = - \int dx'' \gamma(x, x'') \gamma(x'', x')^{N+\sigma-1} \gamma(x'', x')^{N-\sigma} \mathcal{D}(x'', x') \quad (\text{S51})$$

Written in this form these equations indicate the emergent conformal symmetry. This is especially obvious for Eq. S50 that maps onto the  $q$ -SYK Dyson equation,  $q = 2N$ , which is invariant under the conformal group of time reparametrizations  $t \rightarrow \tau$ , e.g. see Refs. [42, 43]

$$t = f(\tau) \quad (\text{S52})$$

$$\tilde{g}(\tau_1, \tau_2) = |f'(\tau_1) f'(\tau_2)|^h g(f(\tau_1), f(\tau_2)) \quad (\text{S53})$$

$$\tilde{\psi}(\tau, x) = |f'(\tau)|^h \psi(t, x) \quad (\text{S54})$$

where  $h = 1/(2N)$  is the temporal conformal dimension, see Eq. S29,  $f'(\tau) \neq 0$  is the derivative of  $f$  in  $\tau$ ,  $g(t, t')$  is a solution of the Dyson Eq. S50,  $\psi(t, x)$  ( $\tilde{\psi}(\tau, x)$ ) is the fermion field whose propagator is  $g(t, t') \gamma(x, x')$  ( $\tilde{g}(\tau, \tau') \gamma(x, x')$ ). The functions  $\tilde{g}(\tau, \tau')$  are also the solutions of the Dyson Eq. S50 given that  $g(t, t')$  is a solution. Therefore, the ansatz solution given by Eq. S24 produces the continuum of other solutions, see Eq. S53, that can be parametrized by an arbitrary function  $f(\tau)$ . All such time reparametrizations  $f(\tau)$  constitute the conformal group of one-dimensional diffeomorphisms. A field theory with conserved conformal symmetry is called conformal field theory. In one-dimensional conformal field theories, the conformal symmetry alone defines the scaling properties of the fermion Green function as well as of the higher order correlation functions [45]. Apart from the emergent conformal symmetry Eq. S50 is also invariant under the  $U(1)$  gauge transformations corresponding to the electromagnetic gauge invariance of the effective Hamiltonian  $V(R)$ , see Eq. 5 in the main text.

Equation S51 is also invariant under the conformal symmetry which is given by the coordinate reparametrizations

$$x = f(X) \quad (\text{S55})$$

$$\tilde{\gamma}(X_1, X_2) = |f'(X_1) f'(X_2)|^l \gamma(f(X_1), f(X_2)) \quad (\text{S56})$$

$$\tilde{\psi}(t, X) = |f'(X)|^l \psi(t, x) \quad (\text{S57})$$

$$\tilde{\mathcal{D}}(X_1, X_2) = |f'(X_1) f'(X_2)|^l \mathcal{D}(f(X_1), f(X_2)) \quad (\text{S58})$$

where  $l$  is the spatial conformal dimension given by Eq. S36, the function  $f$  is different from the one used in Eq. S52,  $f'(X) \neq 0$  stands for the derivative of  $f$  in  $X$ ,  $\gamma(x, x')$  is a solution of Eq. S51,  $\psi(t, x)$  ( $\tilde{\psi}(t, X)$ ) is the fermion field whose propagator is  $g(t, t') \gamma(x, x')$

$(g(t, t')\tilde{\gamma}(X, X'))$ . As in the previous case the ansatz solution given by Eq. S31 generates the continuum of solutions  $\tilde{\gamma}(X, X')$ , see Eq. S56, that can be parametrized by an arbitrary function  $f(X)$ . The functions  $f(X)$  constitute the conformal group of the coordinate diffeomorphisms. In order to satisfy the conformal symmetry, we also had to transform the effective interaction  $\mathcal{D}(x, x') \rightarrow \tilde{\mathcal{D}}(X, X')$ , see Eq. S58, where  $\mathcal{D}(x, x') = \mathcal{D}(x - x')$  is given by Eq. S14 with  $\mathcal{K} = 0$ . According to Eq. S58 the function  $\tilde{\mathcal{D}}(X, X')$  transforms as a propagator of some emergent conformal field of the spatial conformal dimension  $\nu$ , for  $\nu$  see Eq. 8 in the main text. This emergent conformal field is not physical but rather the result of the dimensional reduction from  $D$  spatial dimensions to a single dimension  $x$ . Combining this one-dimensional spatial conformal symmetry with the temporal one, we restore the emergent two-dimensional conformal symmetry of the Dyson Eq. S18. Thus, we reduced the SCBA in the limit of strong interaction to a (1+1)-dimensional, i.e. two-dimensional, conformal field theory.

In this section we have shown that the FSR condition  $\mathcal{K} = 0$  leads to the emergent conformal symmetry in the infrared limit with the fermion Green function that contains no quasiparticles, see Eq. S42. In other words, the infrared physics at the FSR can be described by some two-dimensional conformal field theory. Conformal field theories correspond to fixed points of the renormalization group procedure, i.e. all running coupling constants tend to some fixed value in the infrared limit. In particular, the interaction coupling constant tends to some fixed value in agreement with the SCBA that treats the interaction vertex as a constant. Thus, the emergent conformal symmetry of the SCBA Dyson Eq. S18 makes this approximation exact in the infrared limit.

**Stability of the fixed point.** The Green function given by Eq. S41 is obtained within the strongly interacting limit. In this limit we suppress the spectral single-particle terms, so that the Green function is entirely defined via its self-energy, see Eq. S16. In order to make such assumptions legitimate, we have to check that our solution is stable against small single-particle perturbations that we include via the following Euclidean action

$$S_0 = \int dt dx \sum_{a=1}^{2N} \psi_a^\dagger(t, x) (\partial_t + H_a) \psi_a(t, x) \quad (\text{S59})$$

where  $H_a = -iv_a \partial_x$  is the single-particle Hamiltonian describing the linear electron dispersion near the  $a^{\text{th}}$  Fermi surface,  $v_a$  is the Fermi velocity, and  $x$  is the extended radial coordinate. Such treatment allows us to study crossovers between the non-Fermi-liquid and LFL ground states [21]. Propagators of the fermion fields  $\psi_a(t, x)$  are given by  $G_a(t, x)$ , see Eq. S19. The fields  $\psi_a(t, x)$  are conformal with temporal and spatial conformal dimensions  $h$  and  $l$ , respectively, see Eqs. S54, S57. Rescaling the time and coordinate as  $t \rightarrow t/s$ ,  $x \rightarrow x/s$  leads to  $\psi_a(t, x) \rightarrow s^{-h-l} \psi_a(t/s, x/s)$ . This makes  $S_0$  a relevant perturbation because it rescales as  $S_0 \rightarrow s^\mu S_0$  with  $\mu > 0$

for  $D > 1$

$$\mu = 1 - 2(h+l) = \frac{D+1}{2} - \frac{D+3}{2N} > 0 \quad (\text{S60})$$

At the same time, the interaction contribution to the action that corresponds to the effective Hamiltonian  $V(R)$ , does not renormalize according to the RG argument that we built in the previous section. In fact, the effective two-dimensional conformal field theory that corresponds to the Dyson Eq. S18 can be represented by the following action

$$S_{int} = \int dt dx \psi_1^{L\dagger}(t, x) \dots \psi_N^{L\dagger}(t, x) \psi_{N+1}^R(t, x) \dots \psi_{N+\sigma}^R(t, x) \times \psi_{N+\sigma+1}^L(t, x) \dots \psi_{2N}^L(t, x) \Phi(x) + (L \leftrightarrow R) + h.c. \quad (\text{S61})$$

where  $\Phi(x)$  is the emergent scalar boson with the spatial scaling dimension  $\nu$  whose propagator is  $\mathcal{D}(x)$ ,  $\psi_a^L(t, x)$  ( $\psi_a^R(t, x)$ ) is the effective fermion field in reduced dimensions that corresponds to the incoming (outgoing) s-wave harmonics of the  $D+1$ -dimensional fermion field  $\Psi_a(t, \mathbf{r})$ . The s-wave expansion of the  $\Psi_a(t, \mathbf{r})$  fields is motivated by the s-wave character of the resonant scattering. Of course,  $S_{int}$  contains all terms corresponding to different choices of initial and final states, in Eq. S61 we show only one such choice. The scaling dimension of  $S_{int}$  is then equal to  $2 - 2N(h+l) - \nu = 0$ , where 2 comes from the integration measure,  $-2N(h+l)$  from  $2N$  fermion fields, and  $-\nu$  from the emergent boson. The vanishing scaling dimension agrees with the fact that  $S_{int}$  corresponds to the RG fixed point.

At  $T = 0$  we can go as deep in the infrared limit as needed. Therefore, at some energy scale the relevant single-particle term  $S_0$  will dominate over the fixed interaction contribution. This makes the strong coupling limit that we relied on in our calculations invalid in the deep infrared limit. Therefore, at  $T = 0$  the single-particle physics always dominates over the interaction which restores the LFL in the infrared limit. In other words, the strongly interacting RG fixed point is always unstable at  $T = 0$ . The RG treatment where the single-particle terms are considered as perturbation compared to the interaction term can be found e.g. in Ref. [21].

Strictly speaking, we cannot apply this RG argument at the scales when the single-particle term  $S_0$  becomes comparable with  $S_{int}$ , because  $S_0$  is treated here as a perturbation. However, this argument is still good enough to conclude that the RG fixed point that we have found here is unstable at  $T = 0$  and the strong interaction limit is not justified. In order to make the statement that the LFL is restored in the infrared limit, one had to perform a standard RG procedure where the single-particle term is considered strong while the interaction is treated as perturbation. Here we conjecture that any weak repulsive interaction in Fermi liquids in spatial dimensions  $D > 1$  does not destroy the LFL. In order to make a qualitative change, the interaction has to be strong enough.

So far we have obtained the seemingly negative result that our strong interaction fixed point is unstable at  $T = 0$ . However, here we aim to show that the thermal

fluctuations stabilize quantum criticality. We also derive the characteristic temperature  $T^*$  that corresponds to the crossover between the LFL and the quantum critical state. In case of finite  $T$  the rescaling parameter  $s$  in the infrared limit can only run up to some maximal value  $s(T) = \Lambda/T$ . Given that the single-particle terms are small, the ultraviolet energy scale  $\Lambda$  is provided by the interaction, see Eq. 6 in the main text. The energy scale of the single-particle term is the Fermi energy  $E_F$ , so the strongly interacting limit corresponds to  $\Lambda \gg E_F$ . In the infrared limit the single-particle action  $S_0$ , see Eq. S59, is enhanced by the factor  $s(T)^\mu$ , for  $\mu$  see Eq. S60. This renders typical single-particle energy to  $s(T)^\mu E_F$ . If this scale is still much smaller than the interaction scale  $\Lambda$ , then the strong interaction regime survives in the infrared limit

$$s(T)^\mu E_F \ll \Lambda \quad (\text{S62})$$

This condition means that the quantum criticality survives at finite temperatures  $T \gg T^*$

$$T^* = E_F \left( \frac{E_F}{\Lambda} \right)^\zeta = \frac{E_F}{r_s^{(N-1)\zeta}}, \quad \zeta = \frac{1}{\mu} - 1 = \frac{2-\nu}{N-2+\nu} \quad (\text{S63})$$

where  $\nu$  is given by Eq. 8 in the main text, the interaction parameter  $r_s$  is given by Eqs. 1 and 6 in the main text. In the main text we discuss Eq. S63. In the limit of infinite interaction  $r_s \rightarrow \infty$  we have to reach the quantum criticality even at  $T = 0$ . This is only possible if  $\zeta > 0$ . The positivity of  $\zeta$  automatically results in  $T^* \ll E_F$ . The case when  $\zeta = 0$  is marginal and requires more care. The positivity of  $\zeta$  is equivalent to the constraint for  $N$  given by Eq. 13 in the main text.

Of course, apart from  $S_0$  we also have to check the interaction terms that we omitted in our model. However, these terms are less relevant than the single-particle terms, so we can safely neglect them. This agrees with our assumption that these terms never lead to the breakdown of the LFL but only renormalize the parameters of the free theory.

**Linear response functions.** In this section we make use of the conformal symmetry to demonstrate that the vertex corrections of the linear response functions, such as the dc conductivity and the charge susceptibilities, do not influence the critical exponents. We consider the general case of linear response function  $\chi_{AB}(t, t')$ , where  $A$  and  $B$  are some operators that are placed in the vertices of the response function. Dependence of  $\chi_{AB}$  on the effective spatial coordinates  $x, x'$  can be considered analogously. Here we use the relation between the linear response functions and the four-point Green function  $G^{(IV)}(t_1, t_2; t_3, t_4)$

$$\chi_{AB}(t, t') = \text{Tr} \left( A G^{(IV)}(t, t; t', t') B \right) \quad (\text{S64})$$

where Tr stands for the trace over the index space. It is not important for us how exactly the trace is taken, here we are after the time scaling of  $\chi_{AB}(t, t')$ . The global

conformal symmetry (it consists of the translations, dilatations, special conformal transformations) restricts the four-point Green function to the following form [45]

$$G^{(IV)}(t_1, t_2; t_3, t_4) = F(\tau) \prod_{i < j} t_{ij}^{-\frac{2h}{3}}, \quad \tau = \frac{t_{13}t_{24}}{t_{14}t_{23}} \quad (\text{S65})$$

where  $t_{ij} = t_i - t_j$ ,  $\tau$  is the conformal cross-ratio,  $F(\tau)$  is some function of the cross-ratio,  $h$  is the temporal conformal dimension, see Eq. S29. Equation S65 explicitly separates the pairwise singularities when  $t_i \rightarrow t_j$ . The scaling of  $t_{ij}$  can be found from applying the rescaling of times  $t_i \rightarrow st_i$ . On the one hand, each of the four fields in  $G^{(IV)}$  has conformal dimension  $h$ , so  $G^{(IV)}$  acquires the factor  $s^{-4h}$ . On the other hand, the factor  $s$  comes from each of the six  $t_{ij}$  which fixes their power at  $-2h/3$ . In order to calculate  $\chi_{AB}(t, t')$ , we have to put  $t_1 = t_2 = t$ ,  $t_3 = t_4 = t'$ , see Eq. S64. This leads to the singularities in Eq. S65 as  $t_{12} = t_{34} = 0$ . This problem can be avoided by setting small non-zero  $t_{12}$  and  $t_{34}$  and express them in terms of non-zero  $t_{13} = t_{14} = t_{23} = t_{24} = t - t'$

$$t_{12}t_{34} = \frac{\tau-1}{\tau} t_{13}t_{24} = \frac{\tau-1}{\tau} (t-t')^2 \quad (\text{S66})$$

Then we substitute it in Eq. S65 and take the limit  $t_{12} \rightarrow 0$ ,  $t_{34} \rightarrow 0$

$$G^{(IV)}(t, t; t', t') = \lim_{\tau \rightarrow 1} \left( F(\tau) \left( \frac{\tau-1}{\tau} \right)^{-\frac{2h}{3}} \right) (t-t')^{-4h} \quad (\text{S67})$$

The limit at  $\tau = 1$  yields some constant that we are not interested in. An important consequence of Eq. S67 is the universal scaling of the linear response function with time  $\chi_{AB}(t, t') \propto |t - t'|^{-4h}$ . Dependence of the linear response function on the effective radial coordinate can be deduced similarly. So, the conformal symmetry allows us to restore the time and coordinate scaling of any linear response function at zero temperature  $T = 0$

$$\chi_{AB}(t, x, t', x') \propto |x - x'|^{-4l} |t - t'|^{-4h} \quad (\text{S68})$$

where  $l$  and  $h$  are the spatial and the temporal conformal dimensions, respectively, see Eqs. S29, S36. Notice that this scaling is entirely determined by the conformal symmetry. In particular,  $\chi_{AB}(t, x, t', x')$  contains all corrections to the linear response vertex.

It is worth mentioning that the linear response function with all the vertex corrections neglected has exactly the same scaling

$$\begin{aligned} \chi_{AB}^{(0)}(t, x, t', x') &= \text{Tr} (G(t-t', x-x') A G(t'-t, x'-x) B) \\ &\propto |x - x'|^{-4l} |t - t'|^{-4h} \end{aligned} \quad (\text{S69})$$

In this case the scaling is given directly by the two-point Green function  $G(t, x) = g(t)\gamma(x)$ , see Eqs. S24, S31. Here we suppressed the constants  $C_a$ . This allows us to conclude that the corrections to the linear response vertices do not influence the time and coordinate scaling of the linear response function. In particular, this observation allows us to use Eq. 15 in the main text to identify the temperature scaling of the dc resistivity, even though

that equation does not contain the interaction corrections to the current vertex.

So far we have calculated the linear response function in the  $(t, x)$  representation. However, the coordinate  $x$  is not physical because we introduced it after the dimensional reduction. Let us connect this quantity with the actual dynamical response function (or susceptibility)  $\chi_{AB}(\omega, \mathbf{q})$ . As the interaction correction to the linear response vertex does not affect the time and coordinate scaling of  $\chi_{AB}$ , we can use the bare vertex to analyze the scaling

$$\chi_{AB}^{ab}(\omega, \mathbf{q}) = \int \frac{d\omega d\mathbf{p}}{(2\pi)^{D+1}} \text{Tr}(G_a(w, \mathbf{p}) A G_b(w + \omega, \mathbf{p} + \mathbf{q}) B) \quad (\text{S70})$$

where the Green functions corresponding to  $a^{\text{th}}$  and  $b^{\text{th}}$  Fermi surfaces are considered. There are two distinct sectors for  $\mathbf{q}$ ,  $a$ , and  $b$ . The first one corresponds to the limit  $q \rightarrow 0$  which is only possible if  $a = b$  (momentum conservation). The second sector corresponds to the Kohn anomalies:  $q \approx 2k_a$  if  $a = b$  or  $q \approx |k_a \pm k_b|$  if  $a \neq b$ .

Let us consider the case  $a = b$  and  $q \rightarrow 0$ . In this case the integral over  $\mathbf{p}$  in Eq. S70 is nearly isotropic which allows us to integrate over angles  $d\mathbf{p} \rightarrow \Omega k_a^{D-1} d\delta p_a$ , where  $\Omega$  is the full  $D$ -dimensional solid angle,  $k_a$  is the Fermi momentum of the  $a^{\text{th}}$  Fermi surface, and  $\delta p_a = p - k_a$ , with  $|\delta p_a| \ll k_a$ . In this case the scaling of the dynamical response with  $\omega$  and  $q$  is given (up to a constant) by the Fourier transform of Eq. S68 which we denote with bar,  $\bar{\chi}_{AB}^{aa}(\omega, q)$

$$\chi_{AB}^{aa}(\omega, \mathbf{q}) \propto \bar{\chi}_{AB}^{aa}(\omega, q) \propto q^{4l-1} |\omega|^{4h-1}, \quad q \ll k_F \quad (\text{S71})$$

The conformal dimensions  $h$  and  $l$  are given in Eqs. S29, S36. This result is presented in Eq. 19 in the main text.

In case of Kohn anomalies  $\mathbf{q}$  is a large vector connecting either two antipodal points of one Fermi surface ( $a = b$  and  $q \rightarrow 2k_a$ ) or two radially aligned points on different Fermi surfaces ( $a \neq b$  and  $q \rightarrow |k_a \pm k_b|$ ). The Kohn anomaly corresponds to the resonant radial scattering along the vector  $\mathbf{q}$ . It is clear that there is no resonant scattering far away from the points on the Fermi surface that are connected by  $\mathbf{q}$ . Therefore, the integral over  $\mathbf{p}$  in Eq. S70 is strongly anisotropic and can be estimated as

an integral in the vicinity of these points. In other words, the vectors  $\mathbf{p}$  and  $\mathbf{p} + \mathbf{q}$  in Eq. S70 are nearly aligned. From the dimensional reduction of the self-energy we know that each angular integration restricted by the radial alignment gives the factor  $\delta p^{(D-1)/2}$ , where  $\delta p$  is the momentum mismatch. In this situation  $\delta p = q - q_{ab}^{\pm}$  is the detuning from the resonance, where  $q_{ab}^{\pm} = |k_a \pm k_b|$  if  $a \neq b$ , and  $q_{ab}^+ = 2k_a$  if  $a = b$ . This gives the following divergent Kohn anomaly of any linear response function

$$\begin{aligned} \chi_{AB}^{ab}(\omega, \mathbf{q}) &\propto |q - q_{ab}^{\pm}|^{\frac{D-1}{2}} \bar{\chi}_{AB}^{aa}(\omega, q - q_{ab}^{\pm}) \\ &\propto |q - q_{ab}^{\pm}|^{4l + \frac{D-3}{2}} |\omega|^{4h-1} \end{aligned} \quad (\text{S72})$$

where  $\bar{\chi}_{AB}^{ab}(\omega, \delta p)$  is the Fourier transform of Eq. S68,  $q_{ab}^{\pm} = |k_a \pm k_b|$  if  $a \neq b$ , and  $q_{ab}^+ = 2k_a$  if  $a = b$ . This agrees with Eq. 21 in the main text.

**Comments on the one-dimensional case.** All the results that we provide in the main text are only valid for  $D > 1$  due to the separation of temporal and spatial dynamics, see Eq. S20. In case of  $D = 1$  one has to figure out appropriate linear combinations of  $x$  and  $t$ . Usually, these combinations correspond to the left and right movers.

In the truly one-dimensional case one has to bosonize the effective interaction  $V(R)$  given by Eq. 5 in the main text. We recall that  $V(R)$  contains  $C_{2N}^N$  different terms half of which are conjugates. Right at the FSR that is given by Eq. 2 in the main text  $V(R)$  contains slowly varying terms that can be combined into  $C_{2N}^N$  non-commuting cosines (they can be divided into two groups, with  $C_{2N-1}^N$  terms each, such that terms within the group do not commute while the terms between the two groups do commute). At this point it is not exactly clear how to proceed with such a large number of non-commuting interaction terms. However, due to the competing nature of these cosines we also expect a highly non-trivial quantum critical phase in this case. The case of two non-commuting cosines corresponds to the self-dual sine Gordon model that describes parafermions [46]. Exactly solvable extensions of the sine Gordon model are typically built via extending the underlying symmetry group [47].

- 
- [1] N. W. Ashcroft, N. D. Mermin, *Solid State Physics* (Saunders College, Philadelphia, 1976).
- [2] E. Fermi, Zur quantelung des idealen einatomigen gases. *Z. Phys.* **36**, 902 (1926). doi: 10.1007/BF01400221.
- [3] S.-i. Tomonaga, Remarks on Bloch's method of sound waves applied to many-fermion problems. *Prog. Theor. Phys.* **5**, 544-569 (1950). doi: 10.1143/ptp/5.4.544.
- [4] J. M. Luttinger, An exactly soluble model of a manyfermion system. *J. Math. Phys.* **4**, 1154 (1963). doi: 10.1063/1.1704046.
- [5] D. C. Mattis, E. H. Lieb, Exact solution of a manyfermion system and its associated boson field. *J. Math. Phys.* **6**, 304 (1965). doi: 10.1063/1.1704281.
- [6] L. D. Landau, The theory of a Fermi liquid. *Sov. Phys.-JETP* **3**, 920 (1957).
- [7] K. Seo, V. N. Kotov, B. Uchoa, Ferromagnetic Mott state in twisted graphene bilayers at the magic angle. *Phys. Rev. Lett.* **122**, 246402 (2019). doi: 10.1103/PhysRevLett.122.246402.
- [8] Y. Jiang, X. Lai, K. Watanabe, T. Taniguchi, K. Haule, J. Mao, E. Y. Andrei, Charge order and broken rotational symmetry in magic-angle twisted bilayer graphene. *Nature* **573**, 91-95 (2019). doi: 10.1038/s41586-019-1460-4.
- [9] Y. Cao, V. Fatemi, S. Fang, K. Watanabe, T. Taniguchi, E. Kaxiras, P. Jarillo-Herrero, Unconventional superconductivity in magic-angle graphene superlattices. *Nature*

- 556**, 43-50 (2018). doi: 10.1038/nature26160.
- [10] T. Ando, A. B. Fowler, F. Stern, Electronic properties of two-dimensional systems. *Rev. Mod. Phys.* **54**, 437 (1982). doi: 10.1103/RevModPhys.54.437.
- [11] G. Scappucci, C. Kloeffel, F. A. Zwanenburg, D. Loss, M. Myronov, J.-J. Zhang, S. De Franceschi, G. Katsaros, M. Veldhorst, The germanium quantum information route. arXiv:2004.08133 [cond-mat] (2020).
- [12] W. Heisenberg, Mehrkrperproblem und resonanz in der quantenmechanik. *Z. Phys.* **38**, 411-426 (1926). doi: 10.1007/BF01397160.
- [13] E. Fradkin, *Field Theories of Condensed Matter Physics* (Cambridge University Press, ed. 2, 2013). doi: 10.1017/CBO9781139015509.
- [14] L. D. Landau, I. Y. Pomeranchuk, On the properties of metals at very low temperatures. *Sov. Phys.-JETP* **7**, 379 (1937).
- [15] S. Sachdev, *Quantum Phase Transitions* (Cambridge University Press, ed. 2, 2011). doi: 10.1017/CBO9780511973765.
- [16] P. Coleman, A. J. Schofield, Quantum criticality. *Nature* **433**, 226-229 (2005). doi: 10.1038/nature03279.
- [17] R. Daou, N. Doiron-Leyraud, D. LeBoeuf, S. Y. Li, F. Laliberté, O. Cyr-Choinière, Y. J. Jo, L. Balicas, J.-Q. Yan, J.-S. Zhou, J. B. Goodenough, L. Taillefer, Linear temperature dependence of resistivity and change in the Fermi surface at the pseudogap critical point of a high- $T_c$  superconductor. *Nat. Phys.* **5**, 31-34 (2009). doi: 10.1038/nphys1109.
- [18] B. Keimer, S. A. Kivelson, M. R. Norman, S. Uchida, J. Zaanen, From quantum matter to high-temperature superconductivity in copper oxides. *Nature* **518**, 179-186 (2015). doi: 10.1038/nature14165.
- [19] P. Gegenwart, Q. Si, F. Steglich, Quantum criticality in heavy-fermion metals. *Nat. Phys.* **4**, 186-197 (2008). doi: 10.1038/nphys892.
- [20] O. Parcollet, A. Georges, Non-Fermi-liquid regime of a doped Mott insulator. *Phys. Rev. B* **59**, 5341 (1999). doi: 10.1103/PhysRevB.59.5341.
- [21] D. Chowdhury, Y. Werman, E. Berg, T. Senthil, Translationally invariant non-Fermi-liquid metals with critical Fermi surfaces: solvable models. *Phys. Rev. X* **8**, 031024 (2018). doi: 10.1103/PhysRevX.8.031024.
- [22] R. A. Davison, K. Schalm, J. Zaanen, Holographic duality and the resistivity of strange metals. *Phys. Rev. B* **89**, 245116 (2014). doi: 10.1103/PhysRevB.89.245116.
- [23] S. Sachdev, J. Ye, Gapless spin-fluid ground state in a random quantum Heisenberg magnet. *Phys. Rev. Lett.* **70**, 3339 (1993). doi: 10.1103/PhysRevLett.70.3339.
- [24] M. Dresselhaus, G. Dresselhaus, S. B. Cronin, A. G. S. Filho, *Solid State Properties: From Bulk to Nano* (Springer, Berlin, Heidelberg, ed. 1, 2018). doi: 10.1007/978-3-662-55922-2.
- [25] A. Manchon, H. C. Koo, J. Nitta, S. M. Frolov, R. A. Duine, New perspectives for Rashba spinorbit coupling. *Nat. Mater.* **14**, 871-882 (2015). doi: 10.1038/nmat4360.
- [26] F. Dettwiller, J. Fu, S. Mack, P. J. Weigele, J. C. Egues, D. D. Awschalom, D. M. Zumbühl, Stretchable persistent spin helices in GaAs quantum wells. *Phys. Rev. X* **7**, 031010 (2017). doi: 10.1103/PhysRevX.7.031010.
- [27] A. Kriisa, R. L. Samaraweera, M. S. Heimbeck, H. O. Everitt, C. Reichl, W. Wegscheider, R. G. Mani, Cyclotron resonance in the high mobility GaAs/AlGaAs 2D electron system over the microwave, mm-wave, and terahertz- bands. *Sci. Rep.* **9**, 2409 (2019). doi: 10.1038/s41598-019-39186-2.
- [28] M. -H. Whangbo, E. Canadell, P. Foury, J. -P. Pouget, Hidden Fermi surface nesting and charge density wave instability in low-dimensional metals. *Science* **252**, 96-98 (1991). doi: 10.1126/science.252.5002.96.
- [29] S. Murayama, C. Sekine, A. Yokoyanagi, K. Hoshi, Y. Ōnuki, Uniaxial Fermi-surface nesting and spin-density-wave transition in the heavy-fermion compound Ce(Ru<sub>0.85</sub>Rh<sub>0.15</sub>)<sub>2</sub>Si<sub>2</sub>. *Phys. Rev. B* **56**, 11092 (1997). doi: 10.1103/PhysRevB.56.11092.
- [30] L. Trifunovic, D. Loss, J. Klinovaja, From coupled Rashba electron- and hole-gas layers to three-dimensional topological insulators. *Phys. Rev. B* **93**, 205406 (2016). doi: 10.1103/PhysRevB.93.205406.
- [31] Y. Volpez, D. Loss, J. Klinovaja, Three-dimensional fractional topological insulators in coupled Rashba layers. *Phys. Rev. B* **96**, 085422 (2017). doi: 10.1103/PhysRevB.96.085422.
- [32] A. R. Hamilton, E. H. Linfield, M. J. Kelly, D. A. Ritchie, G. A. C. Jones, M. Pepper, Transition from one- to two-subband occupancy in the 2DEG of back-gated modulation-doped GaAs-Al<sub>x</sub>Ga<sub>1-x</sub>As heterostructures. *Phys. Rev. B* **51**, 17600 (1995). doi: 10.1103/PhysRevB.51.17600.
- [33] Z. W. Zheng, B. Shen, R. Zhang, Y. S. Gui, C. P. Jiang, Z. X. Ma, G. Z. Zheng, S. L. Guo, Y. Shi, P. Han, Y. D. Zheng, T. Someya, Y. Arakawa, Occupation of the double subbands by the two-dimensional electron gas in the triangular quantum well at Al<sub>x</sub>Ga<sub>1-x</sub>N/GaN heterostructures. *Phys. Rev. B* **62**, R7739(R) (2000). doi: 10.1103/PhysRevB.62.R7739.
- [34] J. C. Y. Teo, C. L. Kane, From Luttinger liquid to non-Abelian quantum Hall states. *Phys. Rev. B* **89**, 085101 (2014). doi: 10.1103/PhysRevB.89.085101.
- [35] P. P. Aseev, D. Loss, J. Klinovaja, Conductance of fractional Luttinger liquids at finite temperatures. *Phys. Rev. B* **98**, 045416 (2018). doi: 10.1103/PhysRevB.98.045416.
- [36] P. Stano, J. Klinovaja, A. Yacoby, D. Loss, Local spin susceptibilities of low-dimensional electron systems. *Phys. Rev. B* **88**, 045441 (2013). doi: 10.1103/PhysRevB.88.045441.
- [37] W. Kohn, Image of the Fermi surface in the vibration spectrum of a metal. *Phys. Rev. Lett.* **2**, 393 (1959). doi: 10.1103/PhysRevLett.2.393.
- [38] R. E. Peierls, *Quantum Theory of Solids* (Clarendon, Oxford, 1955).
- [39] M. A. Ruderman, C. Kittel, Indirect exchange coupling of nuclear magnetic moments by conduction electrons. *Phys. Rev.* **96**, 99 (1954). doi: 10.1103/PhysRev.96.99.
- [40] B. Braunecker, P. Simon, D. Loss, Nuclear magnetism and electron order in interacting one-dimensional conductors. *Phys. Rev. B* **80**, 165119 (2009). doi: 10.1103/PhysRevB.80.165119.
- [41] C. P. Scheller, T.-M. Liu, G. Barak, A. Yacoby, L. N. Pfeiffer, K. W. West, D. M. Zumbühl, Possible evidence for helical nuclear spin order in GaAs quantum wires. *Phys. Rev. Lett.* **112**, 066801 (2014). doi: 10.1103/PhysRevLett.112.066801.
- [42] R. Gurau, Notes on Tensor Models and Tensor Field Theories. arXiv:1907.03531v2 [hep-th] (2019).
- [43] S. Sachdev, Bekenstein-Hawking entropy and strange metals. *Phys. Rev. X* **5**, 041025 (2015). doi: 10.1103/PhysRevX.5.041025.

- [44] A. Kruchkov, A. A. Patel, P. Kim, S. Sachdev, Thermoelectric power of Sachdev-Ye-Kitaev islands: probing Bekenstein-Hawking entropy in quantum matter experiments. *Phys Rev. B* **101**, 205148 (2020). doi:10.1103/PhysRevB.101.205148.
- [45] P. H. Ginsparg, Applied Conformal Field Theory. arXiv:9108028v1 [hep-th] (1988).
- [46] P. Lecheminant, A. O. Gogolin, A. A. Nersisyan, Criticality in self-dual sine-Gordon models. *Nucl. Phys. B* **639**(3), 502-523 (2002). doi:10.1016/S0550-3213(02)00474-1.
- [47] I. I. Kogan, B. Tekin, A. Kovner, Deconfinement at  $N > 2$ :  $SU(N)$  Georgi-Glashow model in 2+1 dimensions. *J. High Energy Phys.* **2001**, JHEP05 (2001). doi:10.1088/1126-6708/2001/05/062.